Accelerated Discoveries of Mechanical Properties of Graphene Using Machine Learning and High-Throughput Computation

Zesheng Zhang[1], Yang Hong[2], Bo Hou[3], Zhongtao Zhang[4], Mehrdad Negahban[1], Jingchao Zhang[4*]

[1]Mechanical & Materials Engineering, University of Nebraska-Lincoln, Lincoln, NE 68588, USA

[2]Department of Chemistry, University of Nebraska-Lincoln, Lincoln, NE 68588, USA

[3]Department of Engineering, University of Cambridge, CB3-0FA, Cambridge, UK

[4]Holland Computing Center, University of Nebraska-Lincoln, Lincoln, NE 68588, USA

ABSTRACT

Machine learning (ML) has been vastly used in various fields, but its application in engineering science remains in infancy. In this work, for the first time, different machine learning algorithms and artificial neural network (ANN) structures are used to predict the mechanical properties of single-layer graphene under various impact factors of system temperature, strain rate, vacancy defect and chirality. The predictions include fracture strain, fracture strength and Young's modulus. High throughput computation (HTC) combined with classical molecular dynamics (MD) simulation is used to generate the training dataset for the ML models. It was discovered that both temperature and vacancy defect have negative effects on the predicted properties while strain rate has positive correlations with the prediction results. The stochastic gradient descent (SGD) method could not properly capture the effects of the different impact factors on the mechanical properties of graphene, while k-nearest neighbors (KNN), support vector machine (SVM), decision tree (DT) and ANN provided desirable prediction results. Discoveries in this work provide new perspectives on the study of mechanical properties using state-of-the-art computational methods.

---

[*]Corresponding author. E-mail: zhang@unl.edu (Jingchao Zhang); Tel.: +01-402-472-6400

1. Introduction

The peculiar properties of graphene have attracted enormous attentions from scientists all over the world. Due to the unique 2D structure of graphene, it possesses extraordinary thermal [1-3], optical [4-6] and mechanical [7-9] properties. The measured thermal conductivity of graphene can reach 5000 W/m·K [10] with high electron mobility (2.5×10^5 cm^2/V·s) [11] at room temperature. Graphene and graphene-based heterostructures have been extensively used in thermal interface materials for thermal management in electronic devices. The list of potential applications includes field effect transistors (FET) [12], high-end composite materials [13], electromechanical sensors [14], supercapacitors [15], water desalination membranes [16] and solar cells [17].

One of the most important applications of graphene lies in its implementation in mechanical, civil and aerospace reinforcement structures. Graphene-based nanocomposites provide 2D building blocks assembled in layered structures which can provide superior stiffness, strength and energy dissipation capacities [18]. However, no practical devices from these materials will be possible until the physics at the micro/nanoscale is better understood. The elastic constants of pyrolytic graphite has been determined separately by ultrasonic, sonic resonance, and static test methods [19], in which a Young's modulus of 0.91±0.08 TPa was derived. Using an atomic force microscope (AFM) nanoindentation method, the Young's modulus of a monolayer graphene sheet was measured to be 1.0 TPa, which established graphene as the strongest material ever measured [20]. However, the Young's modulus of the multilayer graphene sheets was extracted as only 0.5 TPa, also using an AFM technique [21]. Using first principles approach, Kudin et al. [22] predicted a Young's modulus of 1.02 TPa, Von Lier et al. [23] reported a Young's modulus of 1.11 TPa, and Konstant et al. [24] obtained a Young's

modulus of graphene at 1.24 TPa. Meanwhile, Liu et al. [25] reported Young's modulus at 1.05 TPa and investigated the chirality effect on phonon instability, which normally corresponds to brittle cleavage fracture. In the past ten years, molecular dynamics (MD) simulation dominates the in-silico tests on the mechanical properties of graphene. A vast effort has been put to investigate the effects of various impact factors on the mechanical properties of graphene, such as the effects of system temperature, strain rate, surface defects and chirality. It has been shown that the shear modulus, shear strength and fracture strain of graphene can be reduced as much as 50% by increasing hydrogen coverage to 30% [26]. Using classical MD simulations, Pei et al. [27] revealed that the elastic modulus, strength and fracture strain of graphene can drop by, respectively, as much as 18%, 43% and 47%, with addition of methyl decorations. The fracture strength, strain and Young's modulus reduce, respectively, by 65.9% and 67.6% and 23.7%, when the temperature increases from 300 K to 2000 K [28]. The decrease of fracture strength and strain with increasing temperature can also be explained from the viewpoint of energy [29]. Zhao et al. [30] proved that temperature plays an important role in determining the fracture strength and strain of graphene, while it does not have a significant effect on Young's modulus until about 1200 K, beyond which the material becomes softer. They also reported that strain rate has little effects on the fracture strength and strain at low temperature, but plays a more prominent role at high temperature.

While the mechanical properties of graphene have been investigated both experimentally and numerically, these studies are, in general, capital intensive and time consuming. Therefore, most focused only on one or two aspects. The inclusion of multiple factors in a single study requires extensive effort and is normally difficult to realize. However, by using well-trained machine learning (ML) models, one can easily obtain results with any combination of factors

within a fraction of a second. Given the rapid development of computational power and the explosion in big data, machine learning has been used to build models in a broad number of fields, including information technology, software engineering, time series forecasting and bioinformatics, whereas its application in the realm of engineering science remains in its infancy [31-33].

In this work, accelerated discoveries of graphene's mechanical properties are realized by the combination of machine learning algorithms and high-throughput computations. Effects of different modulators, such as system temperature, strain rate, single vacancy defect and chiral direction, on the mechanical properties of graphene are explored. This paper is organized as follows. Section 2 presents the different machine learning and neural network structures used, followed by principles of the MD simulation method to extract mechanical properties of graphene, such as fracture strain, fracture strength and Young's modulus. The workflow of using ML and HTC to predict the mechanical properties is also provided. Section 3 presents and discusses the results for different impact factors. The training processes for different ML models are explained and the prediction procedures are clarified in detail here. In the last section, the results are summarized, and the contributions of this work are explained.

2. Computational Methods

Four different machine learning algorithms, *i.e.*, stochastic gradient descent (SGD), k-nearest neighbors (KNN), support vector machine (SVM) and decision tree (DT) were used to train on the mechanical properties of graphene obtained from MD simulations. Mean square errors (MSE) were used to evaluate the performances of different models. The MSE is calculated by

$$MSE(y, \hat{y}) = \frac{1}{n} \sum_{i=0}^{n-1} (y_i - \hat{y}_i)^2 , \qquad (1)$$

where y is the target value, $\hat{y}$ is the predicted value, n is the number of samples and i is the sample index. The fracture strain, fracture strength and Young's modulus were simultaneously modeled to obtain comprehensive understanding of the mechanical properties of graphene. As a result, each machine learning model had three unique outputs. The MSE for each output was calculated separately. As opposed to the batch gradient descent method, at each step the SGD method uses a random instance in the training set to compute the gradient, which makes the algorithm much faster due to the small size of data to manipulate at each iteration [34]. This method is particularly useful on large training datasets since only one instance is stored in the memory at each step. But on the other hand, due to its stochastic nature, the optimized results will bounce around the minimum points and never settle down. Neighbors-based regressions, such as the KNN method, can be used in cases where the target values are continuous rather than discrete variables [35]. Since the fracture strain, fracture strength and Young's modulus should change continuously with variation of different impact factors, KNN may be a perfect modelling strategy for these parameters. The SVM algorithm is very powerful and versatile, and has been extensively used in machine learning studies [36]. The method used in support vector classification can be extended to solve regression problems. In support vector regression, instead of trying to draw the largest possible area between different classes, it tries to fit as many instances as possible within the area. Similar to SVM, DT is also a robust machine learning algorithm that can perform both classification and regression trainings [37]. The objective of DT is to create a model that can predict the target values based on simple splitting rules inferred

4

from the input features. The data profiles can be approximated by a set of if-then-else decision rules which can become fairly complicated as the tree grows deeper.

Artificial neural networks, on the other hand, do not use explicit formula expressions to predict the output based on input information. The neural network is consisted of input, output, as well as hidden layers of neuron units, with each neuron representing a weight to be placed on the input value to transform into something the output layer can use. A schematic of a simple neural network is depicted in Fig. 1.
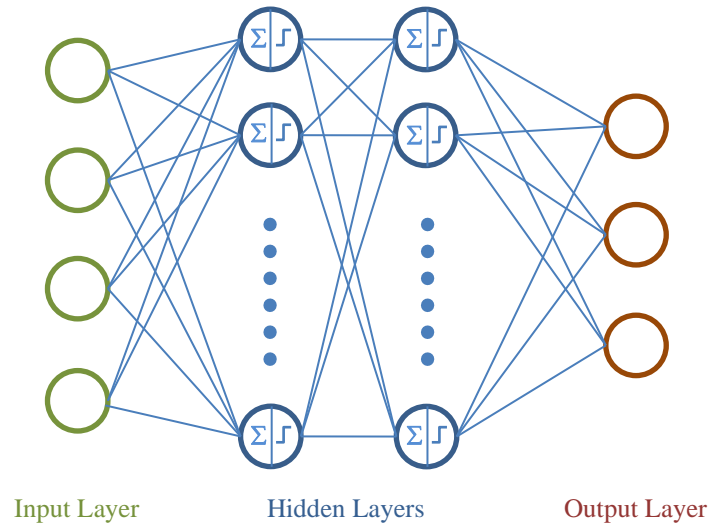

Figure 1. Schematic of a typical neural network structure composed of one input layer, two hidden layers and one output layer.

When the number of hidden layers is ≥ 2, the neural network can be called a deep neural network. Feedforward neural networks are used here, wherein connections between the nodes do not form a cycle. The neural network model is simply a nonlinear function from a set of input variables to a set of output variables controlled by a matrix of adjustable parameters. The objective is to train the network to learn the weights of the neurons that can minimize the MSE.

To suppress the overfitting problem, weight regularizations are generally applied to the neural networking during model training, and the total loss is expresses as

$$L(\vec{w}) = \frac{1}{n}\sum_{i=1}^{n} MSE(y, \hat{y}) + regularizer(\vec{w}),$$ (2)

where $\vec{w}$ is the weight matrix. The weight matrix is updated every step using the gradient descent algorithm

$$\vec{w}^{t+1} = \vec{w}^{t} - \eta\frac{\partial L}{\partial \vec{w}},$$ (3)

where η is the learning rate. The weight updates can be achieved using a local message passing scheme in which information is sent alternately forwards and backwards through the network, which is also known as error backpropagation [38].

The training, validation and testing dataset for different ML models are obtained by MD simulations. All simulations are performed using Large-scale Atomic/Molecular Massively Parallel Simulator (LAMMPS) [39] with the adaptive intermolecular reactive empirical bond order (AIREBO) potential [40]. The time step was set to 0.1 fs. Periodic boundary condition was applied in all directions. A 20 Å vacuum space was created in the out-of-plane z direction to avoid cross-boundary interactions. The graphene sheet without any vacancy defects and the ones with different number of single vacancy defect along armchair direction were created to investigate the effect of single vacancy defects. The temperatures of 1, 10, 100, 300, 600 and 1200 K, and strain rates of 5×10^{-5}, 1×10^{-4}, 2.5×10^{-4}, 5×10^{-4}, 1×10^{-3} and 2.5×10^{-3} ps^{-1} were used for each graphene sheet with or without defects. The strain rates were selected to be small enough to allow the system to respond to the mechanical deformations, while being large

enough for the simulation runs to be computationally feasible. Depending on the stain rates, the stretching process took from 1.2×10^6 to 6×10^7 time steps. The uniaxial tensile deformation was applied in either armchair or zigzag direction to investigate the chirality effect. For each case, five different simulations with different initial conditions were performed and the results were averaged to suppress statistical noise. The graphene sheets were equilibrated for 50 ps at the targeted temperature under the isothermal-isobaric (NPT) ensemble before stretching. The displacement-control method was used at the targeted loading rate with a 0.1 fs time step during stretching. The engineering strain and stress were calculated following the procedure in Zhao's work [41] assuming the thickness of the graphene sheet is 3.35 Å [20].

For each MD simulation case, the fracture strain, fracture strength and Young's modulus were extracted from the strain-stress profiles. A total number of 1440 simulation runs were performed and the results were automatically collected by a MATLAB script. The training dataset was then fed into different ML algorithms for model training. Once the deployment standard was met, the trained ML models could be used to predict the mechanical properties of graphene giving only the impact factors.

3. Results and Discussions

The strain-stress relations in the armchair and zigzag directions at 300K with a strain rate of $5 \times 10^{-4}\,\mathrm{ps^{-1}}$ are shown in Fig. 2. The inset figure shows the chirality effect in the small strain region. As the strain increases, the chirality dependence becomes more distinct. As a result, the graphene sheets fail at 13.0±0.3% and 19.6±0.1% strains, respectively, in armchair and zigzag directions. The associated fracture strengths are 89.4 ± 1.0 GPa and 107.3 ± 0.2 GPa. To investigate the chirality effect on the stiffness, while keeping the fitting portion in the linear

elastic region for both directions, first 2.5% strain range was selected to fit the Young's modulus. The associated Young's moduli were 0.950 ± 0.002 TPa and 0.866 ± 0.006 TPa in armchair and zigzag directions. A list of available experimental and computational results for graphene are shown in Table 1. Our results are in reasonable agreement with these previously published values and indicates the fidelity of the proposed MD model and simulation method. The following uses this MD model to investigate the effects of temperature, strain rate, single vacancy defect, and chirality on the mechanical properties (i.e., fracture strain, fracture strength and Young's modulus) of graphene sheet.

Table 1. Summary of the mechanical properties of graphene

| Authors	Method	Fracture Strain, Armchair/Zigzag (%)	Fracture Strength, Armchair/Zigzag (GPa)	Young's Modulus, Armchair/Zigzag (TPa)
Present	MD	13.0 / 19.6	89.4 / 107.3	0.950 / 0.866
Blakslee et al.[19]	Sonic resonance	-	-	0.91 ± 0.08
Lee et al.[20]	AFM	25	130±10	1.0 ± 0.1
Frank et al.[21]	AFM	-	-	0.5
Kudin et al.[22]	DFT	-	-	1.02
Van Lier et al.[23]	DFT	-	-	1.11
Konstant et al.[24]	DFT	-	-	1.24
Liu et al.[25]	DFT	26.6 / 19.4	121 / 110	1.05
Zhao et al.[41]	MD	13 / 20	90 / 107	1.01 ± 0.03
Ansari et al.[45]	MD	23.3 / 21.8	123 / 127	0.8
Ni et al.[52]	MD	38.1	195	1.13 / 1.05
Tsai et al.[53]	MD	-	-	0.912
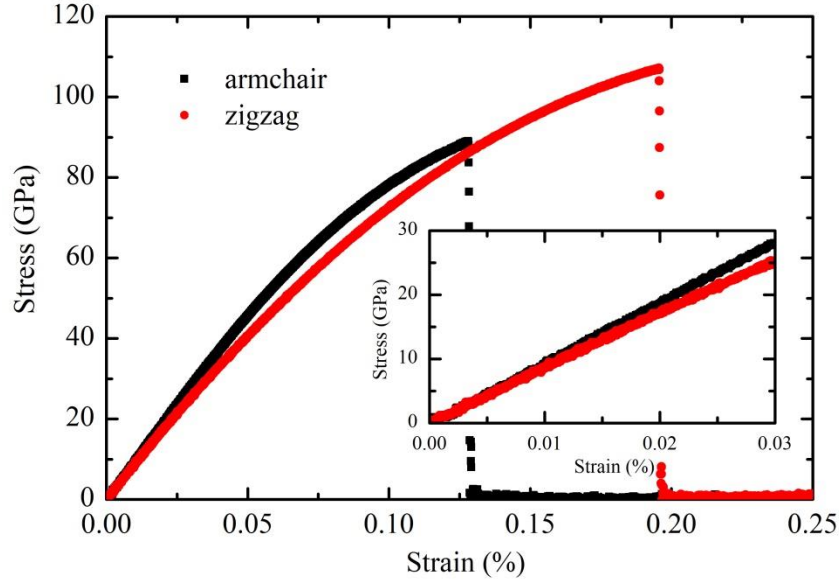
Figure 2. Strain-stress profiles of graphene in armchair and zigzag directions at room temperature with a strain rate of 0.0005 ps^{-1}.

3.1 Effects of temperature and strain rate

The effect of temperature on the fracture strain, strength, and Young's modulus at a strain rate of 5×10^{-4} ps^{-1} are shown in Fig. 3. Overall, the higher temperature deteriorates the mechanical properties of graphene with reduced fracture strain and strength. The two fracture properties decrease nonlinearly with increasing temperature. In the armchair direction, the fracture strain, strength and Young's modulus are more sensitive in the high temperature range than in the low temperature range. To be specific, the fracture strain only decreases 15% during the first two decades of increasing the temperature, which is from 1 K to 100 K, but further drops 40% during the next decade (i.e., from 100 K to 1000 K). The fracture strength decreases 3% during these first two decades, but there is a further drop of 35% in the third decade. The Young's modulus initially drops 1.5% in these first two decades, and then drops another 8.6%

9

during the third decade. The fracture strain and strength in the zigzag direction have similar sensitivities to variation of the temperature as the ones in the armchair direction.
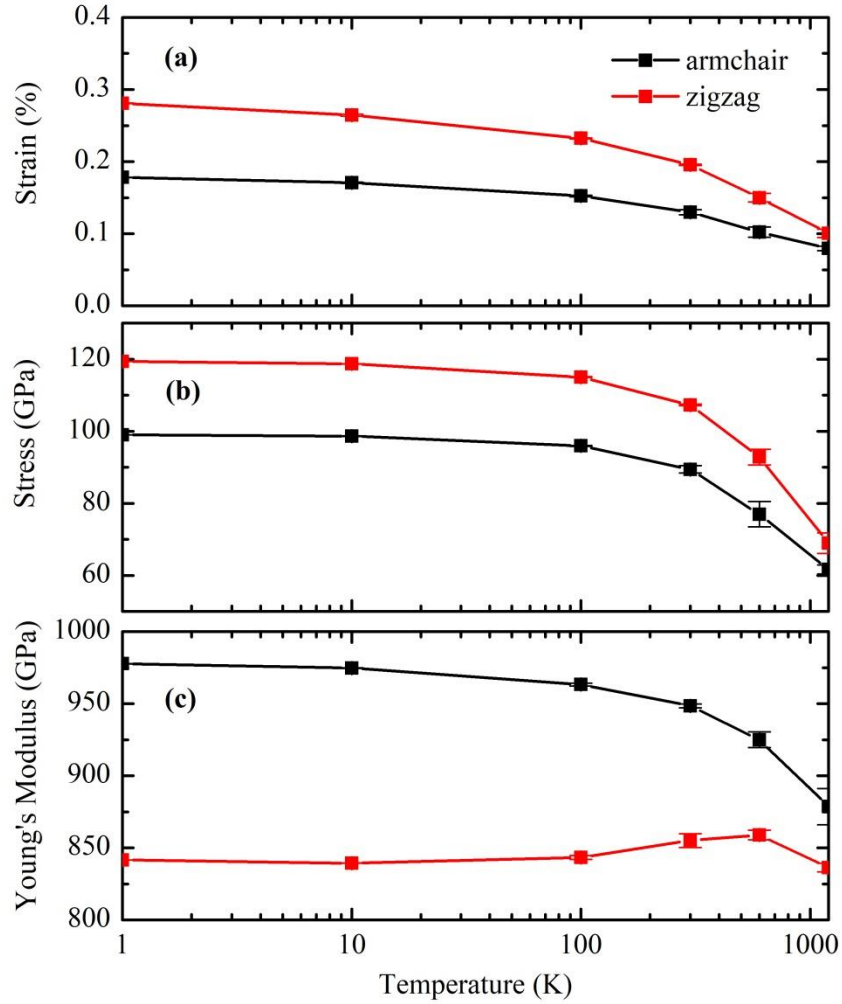

Figure 3. Effects of temperature on (a) fracture strain, (b) fracture strength and (c) Young's modulus of graphene with a strain rate of 0.0005 ps^{-1}.

Compared to the large effect of temperature on the fracture properties, the effect of the strain rate is less significant, especially in the lower temperature range since the system is frozen and cannot promptly respond to the change of the loading rate. Nevertheless, the fracture properties of graphene are enhanced at higher strain rate. As shown in Fig. 4, the fracture strain

in the armchair direction increases with increasing strain rate at all simulation temperatures from 1 K to 1200 K. However, it is clear that the fracture strain is less sensitive to strain rate at lower temperatures than at higher temperatures. For instance, when the strain rate is increased from 5×10^{-5} to 2.5×10^{-3} ps^{-1}, the fracture strain only increases about 1% at 1 K, but increasing about 10% at 1200 K. The fracture strength has a similar trend, where the strength increases by 7% by varying the strain rate from 5×10^{-5} to 2.5×10^{-3} ps^{-1} at 1200 K, but remains unchanged at 1 K. Moreover, the effect of strain rate on the fracture properties in the zigzag direction is similar to the armchair direction, but with different magnitudes, as shown in Fig. 5. One can see that the moduli in the two directions are not changing substantially, even with a 50-fold change in loading rate. This was also observed by others for single-crystalline and polycrystalline graphene [42] and for single-layer and multiple-layer graphene [43].
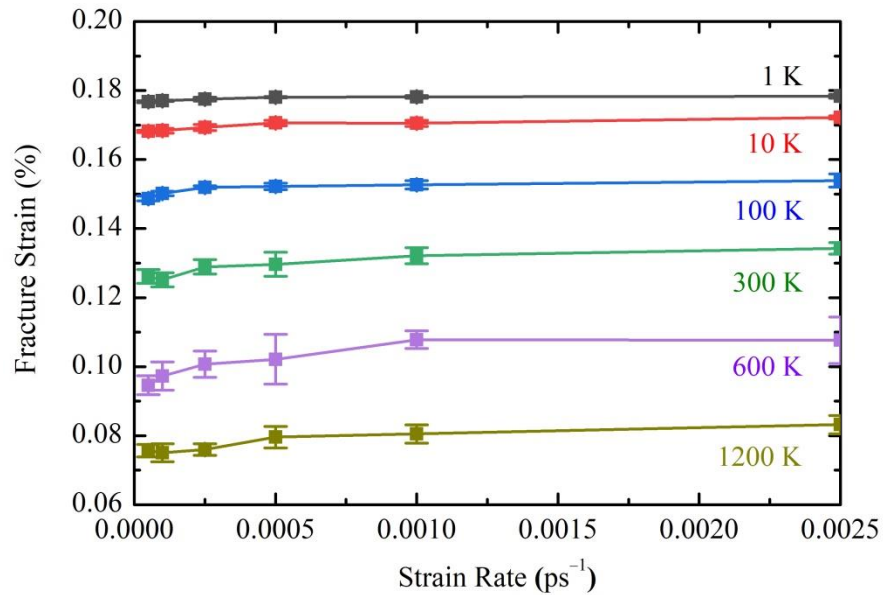

Figure 4. Effects of strain rate on the fracture strain of graphene sheet at different temperature.
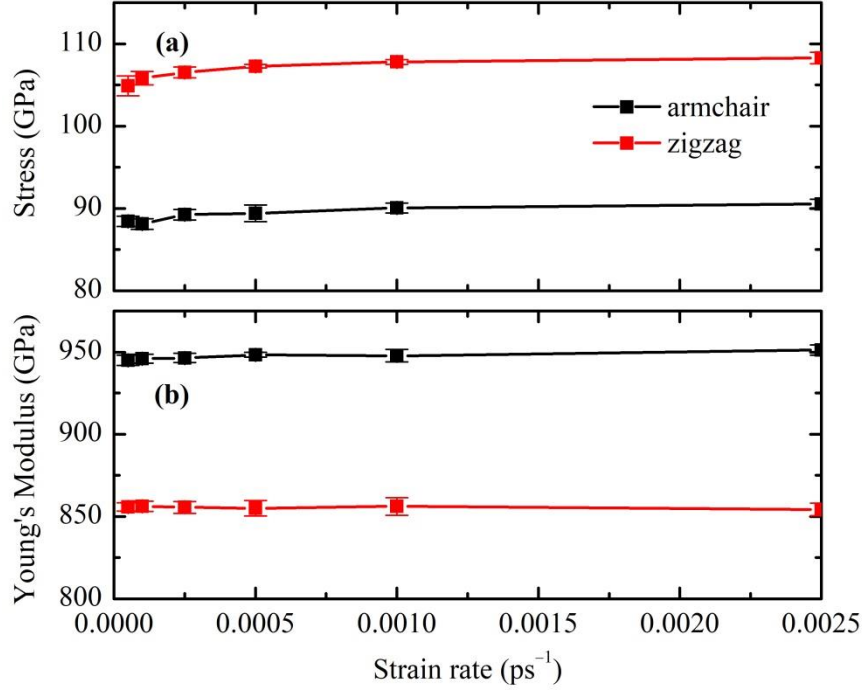
Figure 5. Effects of strain rate on (a) fracture strength and (b) Young's modulus of graphene at room temperature.

3.2 Effects of single vacancy defects

To investigate the effect of single vacancy defects on the mechanical properties of graphene sheet, the graphene sheet without defect and the ones with 1, 2, or 3 single vacancy defects in the center line of zigzag direction and along the armchair direction were created. The influence of the addition of a small number of defects, put here in the form of the addition of vacancies, can substantially affect the response. The effect of the number of single vacancy defects on the fracture strain and strength, and Young's modulus at 300 K for stretching at a strain rate of 0.0005 ps^{-1} are shown in Fig. 6. As indicated, for even a single vacancy defect, the fracture strain and strength in both directions drop substantially (about 29% and 17%, respectively, for fracture strain and strength). It is known that introducing a defect will cause a

stress concentration and thus facilitates easy crack propagation near the defect and result in the graphene sheet failing at low stresses. As discussed in Ansari's work [44], additional reductions of fracture strain and strength occur only when the distance between two defects is smaller than a critical distance (46.86 Å for their system). In addition, introducing single vacancy defects in the presented configuration does not influence the stiffness (i.e., the Young's modulus) of the graphene sheet in either direction, which was also observed in another work [45]. As demonstrated by others [46, 47], the stiffness will reduce only if the density of the defects is significant or the dimension of defect is relatively large comparing to system dimensions.
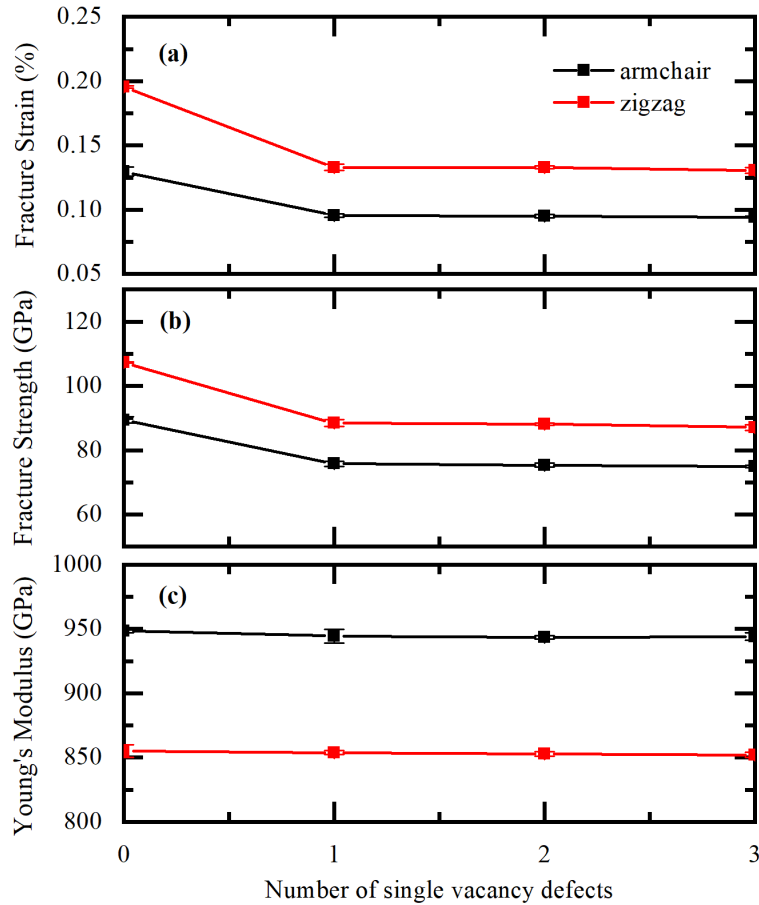

Figure 6. Effects of single atom vacancy defect on (a) fracture strain, (b) fracture strength and (c) Young's modulus of graphene at room temperature with a strain rate of 0.0005 ps^{-1}.

3.3 ML model training and predictions

Based on the MD simulation results, a total of 1440 data points were collected with 4 features (system temperature, strain rate, single vacancy defect and chirality) and 3 target values (fracture strain, fracture strength and Young's modulus) associated with each data point. The dataset was split into 3 portions with, respectively, 64%, 16% and 20% in training, validation, and testing. In order to flag overfitting or selection bias, 10-fold cross-validation is used to test the accuracies of trained models. Once optimal performances were achieved on the validation dataset, the models were employed on the test dataset for a final benchmark. It is worth noting that the dataset was not split randomly but using a stratified method that ensures the most important feature have sufficient impact on the training results. The Pearson's correlation between each pair of features and outputs were calculated and are shown in Fig. 7. The correlation coefficient ranges from −1 to 1, corresponding, respectively, to the strongest negative and positive correlations. As shown in Fig. 7, among the different impact factors, temperature has the strongest effect on the mechanical properties of graphene, which is consistent with the aforementioned MD results. Therefore, stratified splitting was performed based on the temperature distributions. Feature scaling was applied to achieve better training results. All input values were normalized between 0 and 1 to make the feature space evenly distributed. For the SGD method, the stopping criterion was set to 0.001. The l_2 regularization term is used to suppress overfitting. The number of neighbors is 5 for the KNN method. All points in the neighborhood were weighted equally. The Euclidean distance was used to measure the separations between data points. The radial basis function kernel [48] was used in the SVM regressor. The penalty parameter and the loss function cutoff were selected, respectively, as 2000 and 0.001. Once trained, the ML models were used to predict the mechanical properties of

graphene. Prediction results of different models are shown in Fig. 8. All machine learning models except SGD predicted the results reasonably well. Since the SGD method uses a linear kernel, it may be concluded that the mechanical properties of graphene cannot be predicted using linear models for the four impact factors. For other ML models, the predicted fracture strains and strengths closely match the MD simulations results. However, some discrepancies were observed in the Young's modulus, which could be caused by the selections of fitting range.
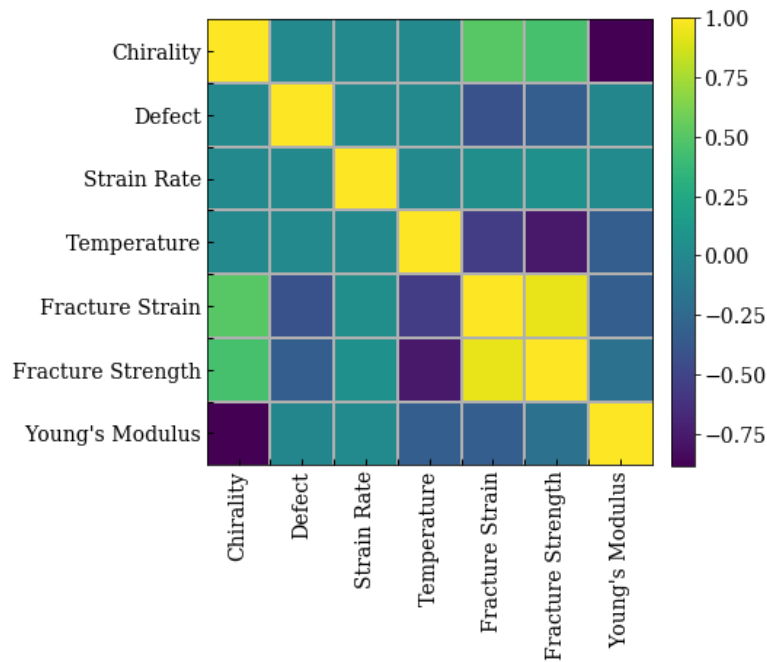

Figure 7. Pearson's correlations between input layer features and output layer targets.

Aside from the ML models used above, four different artificial neural network structures were used. There were, 1 layer with 20 neurons (ANN-20), 1 layer with 40 neurons (ANN-40), 2 layers with 20 neurons each (ANN-20-20) and 2 layers with 40 neurons each (ANN-40-40). The mini-batch gradient descent method was used in the training processes. Instead of computing the gradient based on the full training set or based on only one random instance, the mini-batch gradient descent computes the gradient based on a small set of training instances.
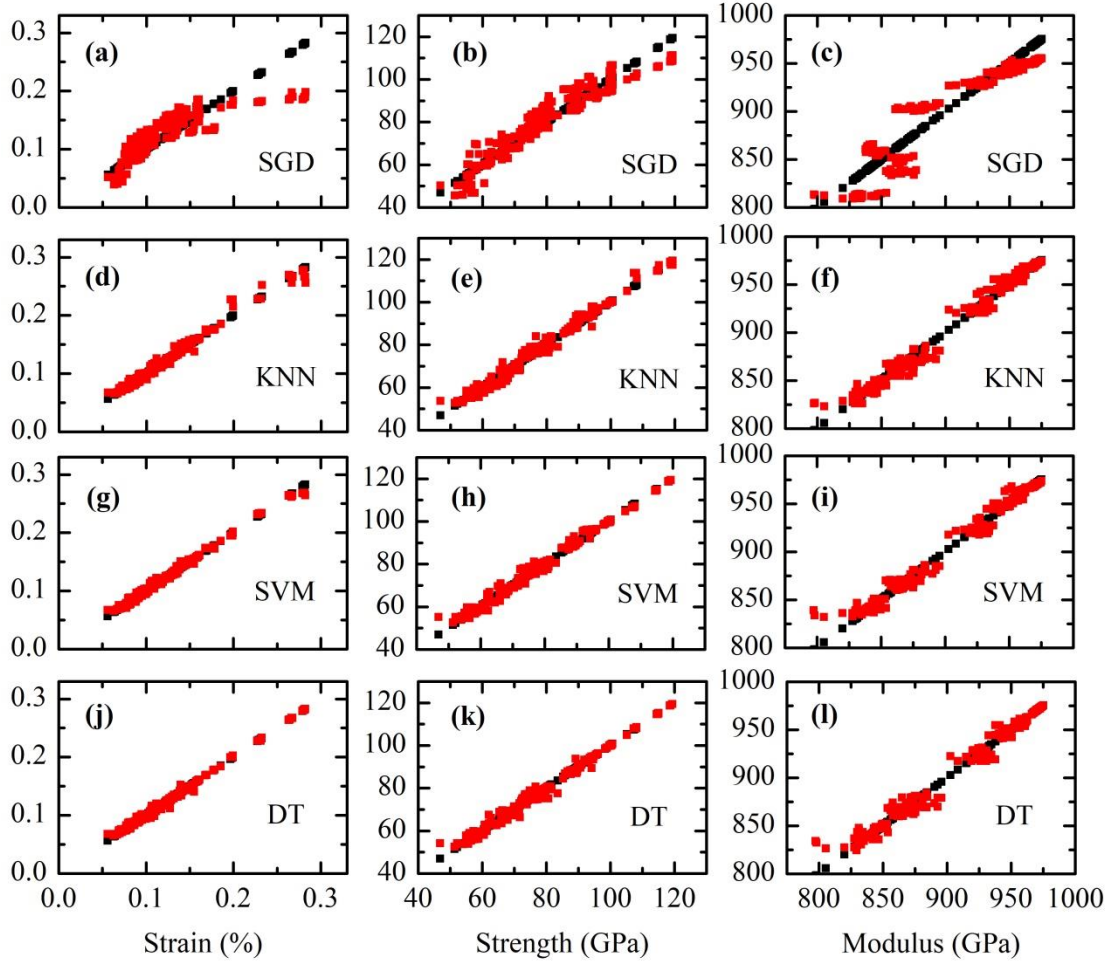
Figure 8. Prediction results of (a)-(c) stochastic gradient descent, (d)-(f) k-nearest neighbors, (g)-(i) support vector machine and (j)-(l) decision tree.

A mini-batch size of 20 was selected in all ANN trainings. The l_2 regularization technique was used to constrain the ANN's connection weights [49]. The dropout regularization [50] was also tested with dropout rates from 0.1 to 0.9, but this did not achieve better performance. Therefore, only l_2 regularization was used in the ANN trainings. The adaptive moment estimation (Adam) optimization [51] method was used to minimize the total loss in the system as expressed in Eqn. 3. The Adam optimization method keeps track of exponentially decaying average of both past gradients and squared gradients. It is worth noting that the regularization

losses must be included in the overall loss in the training process, otherwise they will be neglected. A learning rate of $\eta = 0.001$ was used in all optimizations. The total training epoch was set to 1000, which is long enough to reach optimum training results. Four different activation functions (i.e., linear, logistic, rectified linear unit (ReLU) and exponential linear unit (ELU)) were compared in the ANN models. It was discovered that the ELU activation function gives the best training results and was, thus, selected in all neural network trainings. The ANN training results are shown in Fig. 9. The predicted mechanical properties coincide well with the MD simulations results. To better compare the performances of different ML models, their MSE values on the test dataset are shown in Table 2. Aside from SGD, the performance differences among the different models are subtle.

Table 2. MSE for different algorithms

Algorithms	Fracture Strain (%)	Fracture Strength (GPa)	Young's Modulus (GPa)
SGD	1.6×10^{-3}	27.2	349.7
KNN	3.3×10^{-5}	3.3	38.8
SVM	1.5×10^{-5}	2.3	41.5
DT	9.3×10^{-6}	2.0	43.4
ANN-20	5.4×10^{-5}	4.5	49
ANN-40	3.0×10^{-5}	3.5	43.3
ANN-20-20	2.6×10^{-5}	3.2	39.7
ANN-40-40	1.8×10^{-5}	2.5	41.2

Prediction of mechanical properties using ML was successful, yet more studies are needed. Given the computational power restrictions, only four impact factors were considered here, and the vacancy defect scenario only included single point defects. For each new feature added to the

dataset, the number of instances will increase substantially with the number of attributes in the feature list, which significantly increases the computational effort. In addition, for different ML models, especially the ANN, selection of training parameters is time consuming and it is difficult to capture all possibilities. In this regard, effort should be given to check data integrity and make sure the most important features are included.
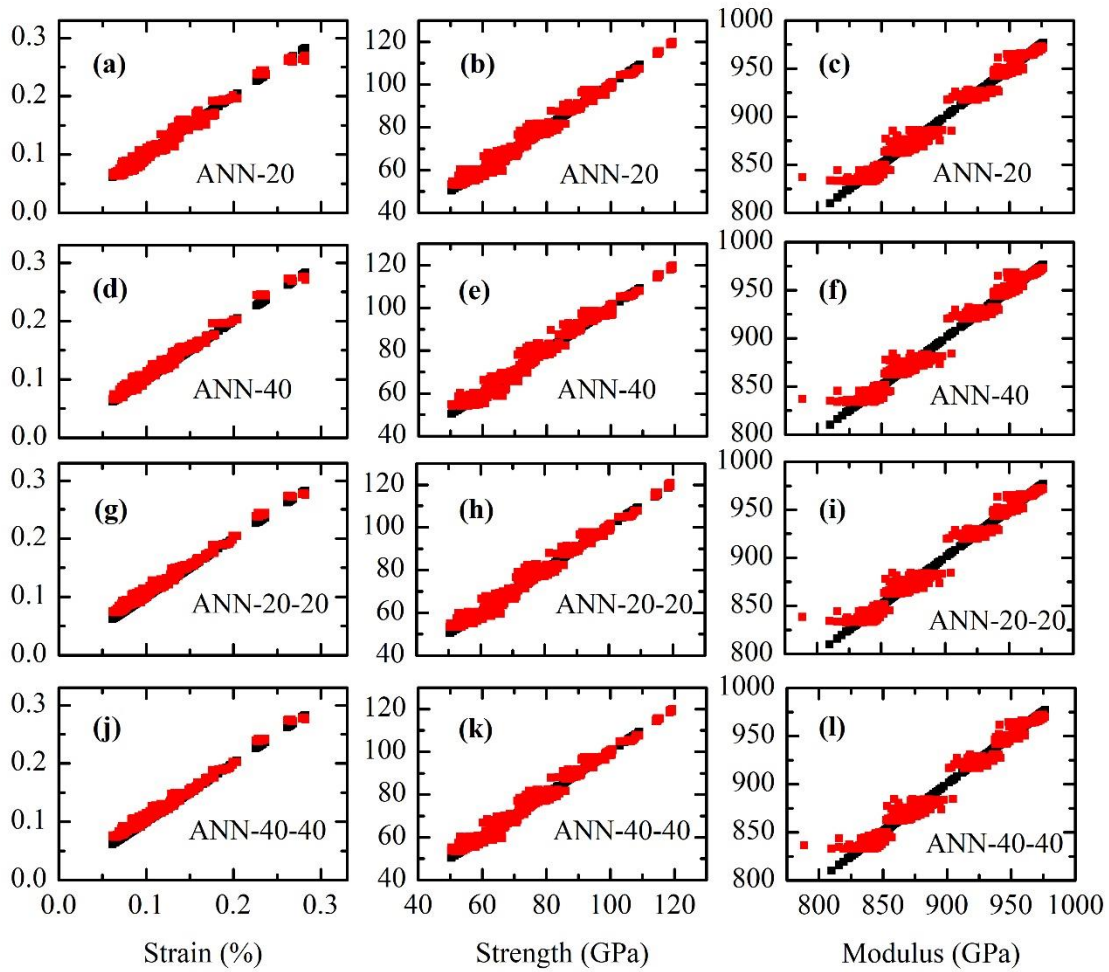

Figure 9. Training results of (a)-(c) 1 layer neural network with 20 neurons, (d)-(f) 1 layer neural network with 40 neurons, (g)-(i) 2 layers neural network with 20 neurons each and (j)-(l) 2 layers neural network with 40 neurons each.

4. Conclusion

Several ML models such as SGD, KNN, SVM, DT and ANN were employed in this work to predict the mechanical properties of graphene using MD obtained datasets. The Young's modulus, fracture strength and fracture strain were investigated in armchair and zigzag directions for the temperature range $1 - 1200$ K, strain rates from 5×10^{-5} to 2.5×10^{-3} ps^{-1} and single vacancy defect from 1 to 3. It was revealed that the mechanical properties of graphene deteriorate with increasing temperature and surface defect, while improved with increasing strain rate. Once trained, the ML models were able to predict the mechanical properties of graphene in a fraction of a second given only the knowledge of system temperature, strain rate, surface defect condition and chiral direction. The MSE of the SGD method was one or two orders of magnitude higher than the other methods, which indicated that it cannot properly model the relationships between the input features and output results. All other models provided excellent prediction results. This work sheds some lights on the explorations of mechanical properties using data-driven approaches and can be applied to a wide range of materials.

References

[1] E. Pop, V. Varshney, A.K. Roy, Thermal properties of graphene: Fundamentals and applications, Mrs Bull 37 (2012) 1273-1281.

[2] J. Zhang, X. Huang, Y. Yue, J. Wang, X. Wang, Dynamic response of graphene to thermal impulse, Physical Review B 84 (2011) 235416.

[3] J. Zhang, F. Xu, Y. Hong, Q. Xiong, J. Pan, A comprehensive review on the molecular dynamics simulation of the novel thermal properties of graphene, RSC Advances 5 (2015) 89415-89426.

[4] L.A. Falkovsky, Optical properties of graphene, J Phys Conf Ser 129 (2008) 012004.

[5] D. Ager, V.A. Vasantha, R. Crombez, J. Texter, Aqueous Graphene Dispersions-Optical Properties and Stimuli-Responsive Phase Transfer, Acs Nano 8 (2014) 11191-11205.

[6] L. Wang, Y.L. Wang, T. Xu, H.B. Liao, C.J. Yao, Y. Liu, Z. Li, Z.W. Chen, D.Y. Pan, L.T. Sun, M.H. Wu, Gram-scale synthesis of single-crystalline graphene quantum dots with superior optical properties, Nat Commun 5 (2014) 5357.

[7] D.G. Papageorgiou, I.A. Kinloch, R.J. Young, Mechanical properties of graphene and graphene-based nanocomposites, Prog Mater Sci 90 (2017) 75-127.

[8] R. Rohini, S. Bose, Extraordinary Improvement in Mechanical Properties and Absorption-Driven Microwave Shielding through Epoxy-Grafted Graphene "Interconnects", Acs Omega 3 (2018) 3200-3210.

[9] Z.L. Xiang, L. Zhang, Y.X. Li, T. Yuan, W.S. Zhang, J.Q. Sun, Reduced Graphene Oxide-Reinforced Polymeric Films with Excellent Mechanical Robustness and Rapid and Highly Efficient Healing Properties, Acs Nano 11 (2017) 7134-7141.

[10] A.A. Balandin, S. Ghosh, W.Z. Bao, I. Calizo, D. Teweldebrhan, F. Miao, C.N. Lau, Superior thermal conductivity of single-layer graphene, Nano Lett 8 (2008) 902-907.

[11] K.S. Novoselov, A.K. Geim, S.V. Morozov, D. Jiang, M.I. Katsnelson, I.V. Grigorieva, S.V. Dubonos, A.A. Firsov, Two-dimensional gas of massless Dirac fermions in graphene, Nature 438 (2005) 197-200.

[12] F. Schwierz, Graphene transistors, Nature Nanotechnology 5 (2010) 487.

[13] J.R. Potts, D.R. Dreyer, C.W. Bielawski, R.S. Ruoff, Graphene-based polymer nanocomposites, Polymer 52 (2011) 5-25.

[14] Q. Liu, J. Chen, Y.R. Li, G.Q. Shi, High-Performance Strain Sensors with Fish-Scale-Like Graphene-Sensing Layers for Full-Range Detection of Human Motions, Acs Nano 10 (2016) 7901-7906.

[15] J.J. Yoo, K. Balakrishnan, J. Huang, V. Meunier, B.G. Sumpter, A. Srivastava, M. Conway, A.L. Mohana Reddy, J. Yu, R. Vajtai, P.M. Ajayan, Ultrathin Planar Graphene Supercapacitors, Nano Lett 11 (2011) 1423-1427.

[16] E.N. Wang, R. Karnik, WATER DESALINATION Graphene cleans up water, Nature Nanotechnology 7 (2012) 552-554.

[17] T. Mahmoudi, Y. Wang, Y.B. Hahn, Graphene and its derivatives for solar cells application, Nano Energy 47 (2018) 51-65.

[18] M.J. Buehler, Nature designs tough collagen: Explaining the nanostructure of collagen fibrils, P Natl Acad Sci USA 103 (2006) 12285-12290.

[19] O.L. Blakslee, D.G. Proctor, E.J. Seldin, G.B. Spence, T. Weng, Elastic Constants of Compression‐Annealed Pyrolytic Graphite, 41 (1970) 3373-3382.

[20] C. Lee, X. Wei, J.W. Kysar, J. Hone, Measurement of the Elastic Properties and Intrinsic Strength of Monolayer Graphene, Science 321 (2008) 385-388.

[21] I.W. Frank, D.M. Tanenbaum, A.M.v.d. Zande, P.L. McEuen, Mechanical properties of suspended graphene sheets, 25 (2007) 2558-2561.

[22] K.N. Kudin, G.E. Scuseria, B.I. Yakobson, C2F, BN, and C nanoshell elasticity from ab initio computations, Physical Review B 64 (2001) 235406.

[23] G. Van Lier, C. Van Alsenoy, V. Van Doren, P. Geerlings, Ab initio study of the elastic properties of single-walled carbon nanotubes and graphene, Chemical Physics Letters 326 (2000) 181-185.

[24] E. Konstantinova, S.O. Dantas, P.M.V.B. Barone, Electronic and elastic properties of two-dimensional carbon planes, Physical Review B 74 (2006) 035417.

[25] F. Liu, P. Ming, J. Li, Ab initiocalculation of ideal strength and phonon instability of graphene under tension, Physical Review B 76 (2007) 064120.

[26] A. Hadizadeh Kheirkhah, E. Saeivar Iranizad, M. Raeisi, A. Rajabpour, Mechanical properties of hydrogen functionalized graphene under shear deformation: A molecular dynamics study, Solid State Communications 177 (2014) 98-102.

[27] P. Qing-Xiang, Z. Yong-Wei, B.S. Vivek, Mechanical properties of methyl functionalized graphene: a molecular dynamics study, Nanotechnology 21 (2010) 115709.

[28] Y.Y. Zhang, Y.T. Gu, Mechanical properties of graphene: Effects of layer number, temperature and isotope, Computational Materials Science 71 (2013) 197-200.

[29] C. Tang, W. Guo, C. Chen, Molecular dynamics simulation of tensile elongation of carbon nanotubes: Temperature and size effects, Physical Review B 79 (2009) 155436.

[30] H. Zhao, N.R. Aluru, Temperature and strain-rate dependent fracture strength of graphene, Journal of Applied Physics 108 (2010) 064321.

[31] H.Y. Yang, Z. An, H.T. Zhou, Y.W. Hou, Application of Machine Learning Methods in Bioinformatics, Aip Conf Proc 1967 (2018) 040015.

[32] J.P. Brown, Machine Learning Applications of Artificial-Intelligence, 1990 Conference on Artificial Intelligence in Petroleum Exploration & Production (1990) 169-176.

[33] W. Zhang, The Application of Machine Learning Algorithms in Data Mining, 2016 International Conference on Information Engineering and Communications Technology (Iect 2016) (2016) 521-527.

[34] H. Robbins, S. Monro, A Stochastic Approximation Method, Ann Math Stat 22 (1951) 400-407.

[35] N.S. Altman, An Introduction to Kernel and Nearest-Neighbor Nonparametric Regression, Am Stat 46 (1992) 175-185.

[36] C. Cortes, V. Vapnik, Support-Vector Networks, Mach Learn 20 (1995) 273-297.

[37] D. Kalles, T. Morris, Efficient incremental induction of decision trees, Mach Learn 24 (1996) 231-242.

[38] D.E. Rumelhart, G.E. Hinton, R.J. Williams, Learning Representations by Back-Propagating Errors, Nature 323 (1986) 533-536.

[39] S. Plimpton, Fast Parallel Algorithms for Short-Range Molecular Dynamics, Journal of Computational Physics 117 (1995) 1-19.

[40] S.J. Stuart, A.B. Tutein, J.A. Harrison, A reactive potential for hydrocarbons with intermolecular interactions, 112 (2000) 6472-6486.

[41] H. Zhao, K. Min, N.R. Aluru, Size and Chirality Dependent Elastic Properties of Graphene Nanoribbons under Uniaxial Tension, Nano Lett 9 (2009) 3012-3015.

[42] M.Q. Chen, S.S. Quek, Z.D. Sha, C.H. Chiu, Q.X. Pei, Y.W. Zhang, Effects of grain size, temperature and strain rate on the mechanical properties of polycrystalline graphene – A molecular dynamics study, Carbon 85 (2015) 135-146.

[43] H. Li, H. Zhang, X. Cheng, The effect of temperature, defect and strain rate on the mechanical property of multi-layer graphene: Coarse-grained molecular dynamics study, Physica E: Low-dimensional Systems and Nanostructures 85 (2017) 97-102.

[44] R. Ansari, B. Motevalli, A. Montazeri, S. Ajori, Fracture analysis of monolayer graphene sheets with double vacancy defects via MD simulation, Solid State Communications 151 (2011) 1141-1146.

[45] R. Ansari, S. Ajori, B. Motevalli, Mechanical properties of defective single-layered graphene sheets via molecular dynamics simulation, Superlattices and Microstructures 51 (2012) 274-289.

[46] M. Neek-Amal, F.M. Peeters, Linear reduction of stiffness and vibration frequencies in defected circular monolayer graphene, Physical Review B 81 (2010) 235437.

[47] J.R. Xiao, J. Staniszewski, J.W. Gillespie, Fracture and progressive failure of defective graphene sheets and carbon nanotubes, Composite Structures 88 (2009) 602-609.

[48] Y.-W. Chang, C.-J. Hsieh, K.-W. Chang, M. Ringgaard, C.-J. Lin, Training and testing low-degree polynomial data mappings via linear SVM, Journal of Machine Learning Research 11 (2010) 1471-1490.

[49] A.E. Hoerl, R.W. Kennard, Ridge regression: Biased estimation for nonorthogonal problems, Technometrics 42 (2000) 80-86.

[50] N. Srivastava, G. Hinton, A. Krizhevsky, I. Sutskever, R. Salakhutdinov, Dropout: A Simple Way to Prevent Neural Networks from Overfitting, Journal of Machine Learning Research 15 (2014) 1929-1958.

[51] D. Kingma, J. Ba, Adam: A Method for Stochastic Optimization, 3rd International Conference for Learning Representations (2015) arXiv:1412.6980.

[52] Z. Ni, H. Bu, M. Zou, H. Yi, K. Bi, Y. Chen, Anisotropic mechanical properties of graphene sheets from molecular dynamics, Physica B: Condensed Matter 405 (2010) 1301-1306.

[53] J.-L. Tsai, J.-F. Tu, Characterizing mechanical properties of graphite using molecular dynamics simulation, Materials & Design 31 (2010) 194-199.